

Uncovering New Higgses in the LHC Analyses of Differential $t\bar{t}$ Cross Sections

Sumit Banik^{a,b} Guglielmo Coloretti^{Ⓜa,b} Andreas Crivellin^{Ⓜa,b} Bruce Mellado^{c,d}

^aPhysik-Institut, Universität Zürich, Winterthurerstrasse 190, CH-8057 Zürich, Switzerland

^bPaul Scherrer Institut, CH-5232 Villigen PSI, Switzerland

^cSchool of Physics and Institute for Collider Particle Physics, University of the Witwatersrand, Johannesburg, Wits 2050, South Africa

^diThemba LABS, National Research Foundation, PO Box 722, Somerset West 7129, South Africa

E-mail: sumit.banik@psi.ch, guglielmo.coloretti@physik.uzh.ch,
andreas.crivellin@psi.ch, bmellado@mail.cern.ch

ABSTRACT: Statistically significant tensions between the Standard Model (SM) predictions and the measured lepton distributions in differential top cross-sections emerged in LHC Run 1 data and became even more pronounced in Run 2 analyses. Due to the level of sophistication of the SM predictions and the performance of the ATLAS and CMS detectors, this is very remarkable. Therefore, one should seriously consider the possibility that these measurements are contaminated by beyond-the-SM contributions. In this article, we use the differential lepton distributions from the latest ATLAS $t\bar{t}$ analysis to study a new physics benchmark model motivated by existing indications for new Higgses: a new scalar H is produced via gluon fusion and decays to S' (95 GeV) and S (152 GeV), which subsequently decay to $b\bar{b}$ and WW , respectively. In this setup, the total χ^2 is reduced, compared to the SM, resulting in $\Delta\chi^2 = 34$ to $\Delta\chi^2 = 158$, corresponding to a significance of 5.8σ to 13σ , depending on the SM simulation used. Notably, allowing m_S to vary, the combination of the distributions points towards $m_S \approx 150$ GeV, which is consistent with the existing $\gamma\gamma$ and WW signals, rendering a mismodelling of the SM unlikely. Averaging the results of the different SM predictions, $\sigma(pp \rightarrow H \rightarrow SS') \times \text{Br}(S \rightarrow WW) \times \text{Br}(S' \rightarrow bb) \approx 9\text{pb}$ is preferred. Assuming that S' is SM-like, the 95 GeV $\gamma\gamma$ excess can be explained if S decays dominantly to W bosons. That latter suggests that S is the neutral component of the $SU(2)_L$ triplet with hypercharge 0.

Contents

1	Introduction	1
2	Analysis and Results	3
3	Simplified Model Analysis	6
4	Conclusions	8
A	Additional Differential Distributions	11

1 Introduction

The known fundamental constituents of matter and their interactions (excluding gravity) are described by the Standard Model (SM) of particle physics. It has been successfully tested and verified by a plethora of measurements [1] with the discovery of the Brout-Englert-Higgs boson [2–5] at the LHC [6, 7] providing its last missing ingredient. Furthermore, this 125 GeV boson has properties and decay rates [8, 9] in agreement with the SM expectations.

Nonetheless, a multitude of new physics models predicts the existence of new Higgses (i.e. scalars that are uncharged under the strong force). Such models are viable if the SM Higgs signal strengths are not significantly altered and their contribution to the ρ parameter ($\rho = m_Z^2/(m_W^2/\cos^2\theta_W)$) is sufficiently small (i.e. custodial symmetry is approximately respected). In fact, the global average of the W -boson mass measurements [10–13] even points to a small additional violation of custodial symmetry with a significance of 3.5σ [14]. This can be explained by various extensions of the SM scalar sector [15]. In particular, the $SU(2)_L$ triplet with hypercharge 0 is an interesting option for explaining the W mass since it predicts a necessarily positive shift, in agreement data.

Dedicated searches for additional Higgs bosons at the LHC have been mostly performed inclusively or with a limited number of topologies, such that significant regions of the phase space remain unexplored. In particular, associated production received relatively little attention. Nonetheless, indications for new Higgses at the electroweak (EW) scale with masses around 95 GeV [16–20] and 152 GeV [21] arose, with global significances of 3.8σ and 4.9σ [22, 23], respectively. In particular, the existence of a 152 GeV boson is also motivated by the “multi-lepton anomalies” [24–27]. These are processes involving multiple leptons and missing energy, with and without (b -)jets, where deviations from the SM expectations have been observed over the last years. Processes with such signatures (in the SM) include WW , WWW , Wh , tW , $t\bar{t}$, $t\bar{t}W$ and $t\bar{t}t\bar{t}$ (see Ref. [27] and references therein). In particular, WW signals are compatible with, or even suggest, a mass of ≈ 150 GeV [28, 29].

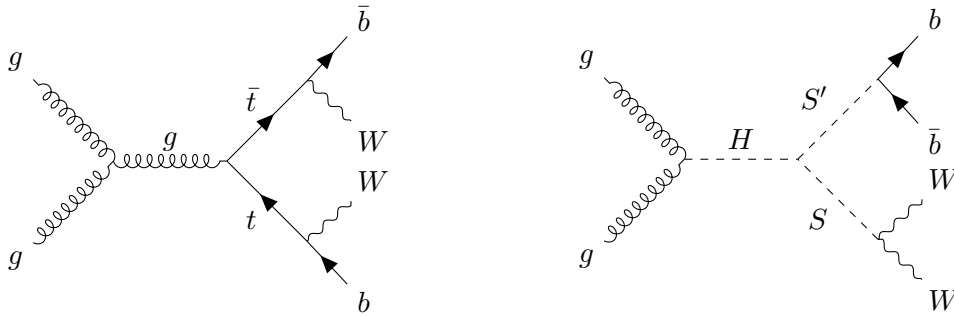


Figure 1. Feynman diagrams showing the leading SM contribution to top pair production and decay as well as the NP signal in our benchmark model contaminating the measurement of $t\bar{t}$ differential distributions.

Here, we will study the statistically most significant multi-lepton excess encoded in the latest ATLAS analysis of the $t\bar{t}$ differential cross-sections [30]. Differential lepton distributions (from leptonic W decays) are advantageous in this context, since the total $t\bar{t}$ cross-section is large and very sensitive to QCD corrections [31–34]. Such differential measurements have been performed by ATLAS [30, 35, 36] and CMS [37, 38]. The ATLAS analysis [30] of $t\bar{t}$ does not only provide the invariant di-lepton mass ($m^{e\mu}$) and the angle between the leptons ($\Delta\phi^{e\mu}$), but also contains an extensive analysis of the different SM predictions using various combinations of Monte Carlo (MC) simulators.¹ Importantly, Ref. [30] concluded that: “No model (SM simulation) can describe all measured distributions within their uncertainties.” Due to the level of rigour and sophistication of the LHC simulations [40, 41] and the performance of the ATLAS and CMS detectors [42–44], this very significant disagreement in a high-statistics measurement including leptons is remarkable.

Therefore, the possibility that NP contaminates the measurement of this SM process should be considered seriously. For the decay $t \rightarrow Wb$ with $W \rightarrow \ell\nu$, the experimental signature of top pair production is opposite-sign different-flavour (to reduce the Z, γ induced background) di-leptons with one or more b -jets. Because the deviations from the SM predictions are most pronounced at low invariant masses of the $e-\mu$ system ($m^{e\mu}$) and small transverse momenta, this points towards an electroweak (EW) scale extension of the SM. For such a beyond-the-SM explanation, light new particles are needed, which are both the source of bottom quarks and of opposite-sign different flavour di-leptons (or are at least produced in association with them). Since the excess is not localized in $m^{e\mu}$, this excludes the direct decay of a new particle to $e\mu$. Furthermore, the broad excess in WW at low masses [29, 45, 46] suggests a new scalar decaying to W bosons. Finally, since a SM-like Higgs with a mass below ≈ 100 GeV naturally decays dominantly to bottom quarks, this hints towards the decay chain $pp \rightarrow H \rightarrow SS'$ with $S \rightarrow WW$ and $S' \rightarrow b\bar{b}$ with $m_{S'} = 95$ GeV and $m_S = 152$ GeV, motivated by the respective hints for narrow

¹Note that the CMS analysis of $t + W$ [39] is less precise but consistent with the ATLAS findings [24]. Furthermore, note that for the $m_{t\bar{t}}$ distribution, we need the W bosons to decay hadronically, which is, however, much less precise than the leptonic distributions.

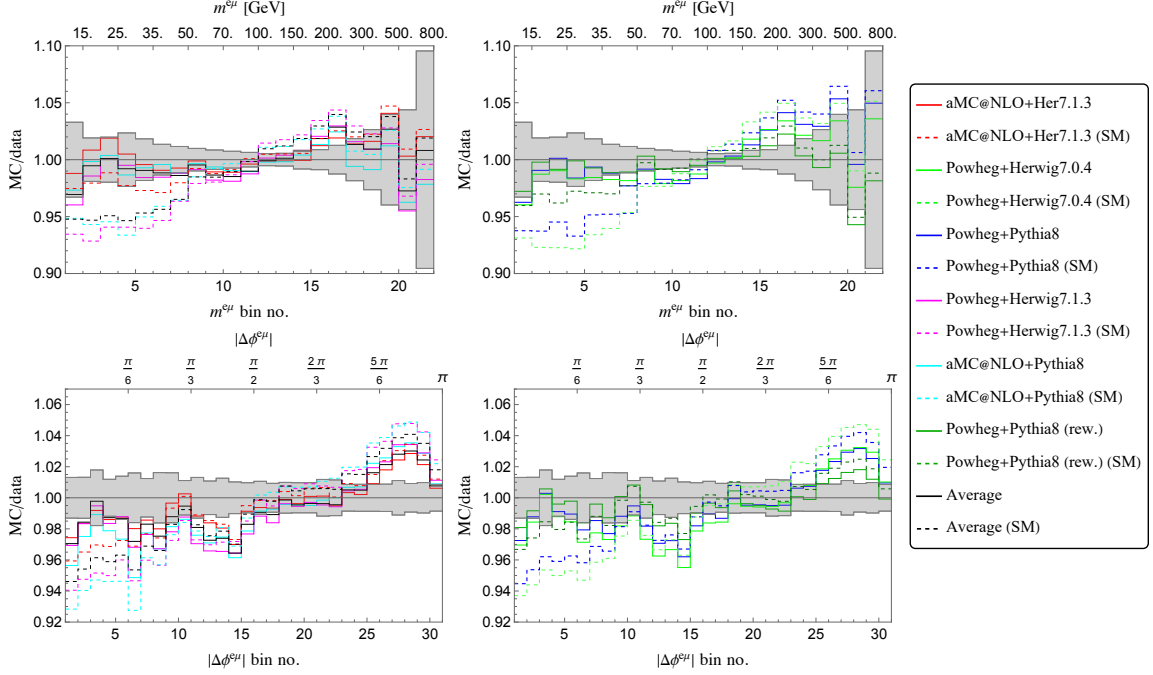


Figure 2. The dashed colored lines show six different SM predictions (MC) normalized to data given in Ref. [30]. The solid lines include the NP contribution from our benchmark model obtained by a combined global fit to $m^{e\mu}$ and $\Delta\phi^{e\mu}$ data. The black lines are obtained by averaging the six predictions and the grey band shows the total uncertainty (systematic and statistical). One can see that the agreement between theory and experiment is significantly increased by adding a NP effect.

resonances.² The Feynman diagram giving the leading contribution in the SM and the one generating the potential NP contamination of our simplified NP model are shown in Fig. 1.

2 Analysis and Results

ATLAS [30] considered six different SM simulations as given in Table 1. In these setups, they predicted differential $t\bar{t}$ distributions, including the invariant mass of the electron-muon pair ($m^{e\mu}$), the sum of the energies $E^e + E^\mu$, the angle between the leptons ($|\Delta\phi^{e\mu}|$), the sum of transverse momentum of the leptons ($p_T^e + p_T^\mu$) and the pseudo-rapidity of the lepton system (η). Here, we will focus on $m^{e\mu}$ and $|\Delta\phi^{e\mu}|$, as they have a fine binning and show the most significant deviations from the SM predictions.³ However, we will later predict the other different distributions to show the consistency of the NP explanation.

²Note that this parameter space is not covered by non-resonant Higgs pair analyses (which aim at higher transverse momenta) or searches for supersymmetric particles like sleptons or charginos (which require more missing energy).

³The high mass region for $m^{e\mu}$ could in general be relevantly affected by EW corrections. However, Ref. [47] found that at low masses, where the discrepancies are most pronounced, their impact is small. We check that excluding the high-mass bins from the fit would have a very small impact.

	$m^{e\mu}$				$\Delta\phi^{e\mu}$				$m^{e\mu} + \Delta\phi^{e\mu}$				
	χ_{SM}^2	χ_{NP}^2	σ_{NP}	Sig.	χ_{SM}^2	χ_{NP}^2	σ_{NP}	Sig.	χ_{SM}^2	χ_{NP}^2	σ_{NP}	Sig.	m_S [GeV]
Powheg+Pythia8	146	50	10pb	9.8 σ	183	73	11pb	10.5 σ	213	102	9pb	10.5 σ	143-156
aMC@NLO+Herwig7.1.3	31	13	4pb	4.2 σ	96	38	8pb	7.6 σ	102	68	5pb	5.8 σ	--
aMC@NLO+Pythia8	89	14	9pb	8.7 σ	277	83	15pb	14.0 σ	291	163	10pb	11.3 σ	148-157
Powheg+Herwig7.1.3	138	32	10pb	10.3 σ	245	93	13pb	12.3 σ	261	126	10pb	11.6 σ	149-156
Powheg+Pythia8 (rew)	40	12	5pb	5.3 σ	54	26	6pb	5.3 σ	69	35	5pb	5.8 σ	--
Powheg+Herwig7.0.4	186	41	12pb	12.0 σ	263	99	14pb	12.8 σ	294	126	12pb	13.0 σ	149-156
Average	93	23	8pb	8.4 σ	172	63	11pb	10.4 σ	182	88	9pb	9.6 σ	143-157

Table 1. χ^2 values, preferred cross-section (σ_{NP}) significance (Sig.) etc. for the individual $m^{e\mu}$ and $|\Delta\phi^{e\mu}|$ distributions and the combined fit to them for the six different SM simulations and their average. The χ_{NP}^2 is for our benchmark scenario with $m_S \approx 152$ GeV while the m_S gives the preferred range of it from the fit, assuming it to be a free parameter. A dash in the m_S column means that the preferred 1σ range is wider than 140 GeV–160 GeV. Note that the cross section preferred by $m^{e\mu}$ and $|\Delta\phi^{e\mu}|$ individually are in very good agreement with each other. The preferred NP cross-section σ_{NP} is given for $\text{Br}[S' \rightarrow b\bar{b}] \approx 100\%$ and $\text{Br}[S \rightarrow WW] \approx 100\%$.

The main input for our analysis is thus Fig. 10 and 11 in Ref. [30], showing the ratio of expected events within the SM (MC) over measured events (data) per bin i , $\text{MC}|_i/\text{data}|_i = x_i$, as well as the corresponding Tables 21 and 24 where the normalized cross sections and the (relative) systematic and statistical uncertainties for each bin (δ_i) are given. Note that ATLAS normalized the differential cross-section to the total one such that the resulting χ^2 value is minimized. In particular, $m^{e\mu}$ is given in 21 bins between $\{0.0, 15.0, 20.0, 25.0, 30.0, 35.0, 40.0, 50.0, 60.0, 70.0, 85.0, 100.0, 120.0, 150.0, 175.0, 200.0, 250.0, 300.0, 400.0, 500.0, 650.0, 800.0\}$ GeV. As the binning for low values of $m_{e\mu}$ is relatively thin, we display the data in Fig. 2 with equal size for all bins to give also optically equal weight to each of them. For $|\Delta\phi^{e\mu}|$ each bin corresponds to an angle of $\pi/30$ and we therefore have 30 bins.

In order to obtain the SM prediction for each bin (and thus x_i) for the different distributions, ATLAS generated $t\bar{t}$ samples with several different matrix element generators, parton shower, and fragmentation simulations. In particular, the nominal sample was obtained using Powheg Box [48–50] with NNPDF3.0 PDF [51] interfaced with Pythia 8.230 [52, 53]. Alternative simulations used MADGRAPH_AMC@NLO [54] (aMC@NLO) with NNPDF2.3 PDF [55] for the event generation or Powheg Box interfaced with Herwig 7.0.4 [56, 57] or 7.1.3 [58]. In the relevant plots the following six different options are shown (using the same colour coding as in Ref. [30]):

- aMC@NLO+Herwig7.1.3
- Powheg+Herwig7.0.4
- Powheg+Pythia8
- Powheg+Herwig7.1.3
- aMC@NLO+Pythia8
- Powheg+Pythia8 (rew.)

In the last case, the p_T of the top quark was reweighted using the kinematics of the top

quarks after initial- and final-state radiation using next-to-next-to-leading order QCD with next-to-leading EW corrections [59].⁴ The values of x_i , are unfortunately not yet available in numerical form and we thus obtained them by digitizing the lower panels of Fig. 10 and 11 using WebPlotDigitizer v4.6 [62] with the integrated automatic tool. The results of this extraction for $m^{e\mu}$ and $|\Delta\phi^{e\mu}|$ are shown in Fig. 2 as dashed lines.

There are two main sources of correlations. First, there is the correlation between events in the $m^{e\mu}$ bins and in $|\Delta\phi^{e\mu}|$ bins since they are overlapping (i.e. not mutually exclusive). To estimate this, we simulated 1600k events of $pp \rightarrow t\bar{t}$ in the SM with MadGraph5aMC@NLO [54], Pythia8.3 [53], and Delphes [63]. Let N_i^m ($N_\alpha^{\Delta\phi}$) be the number of events in the bin i^{th} (α^{th}) of $m^{e\mu}$ ($\Delta\phi^{e\mu}$), disregarding the $\Delta\phi^{e\mu}$ ($m^{e\mu}$) values. $N_{i\alpha}$ denotes the number of events that are both within i^{th} bin of $m^{e\mu}$ and the α^{th} bin of $\Delta\phi^{e\mu}$. The correlation matrix between $m^{e\mu}$ and $\Delta\phi^{e\mu}$ is then given by

$$\rho_{i\alpha} = \frac{\delta_i \delta_\alpha N_{i\alpha}}{\sqrt{\sum_j N_j^m} \sqrt{\sum_\beta N_\beta^{\Delta\phi}}}. \quad (2.1)$$

The second source leading to a correlation is due to the normalization of the distributions to the total cross-section. Within a single distribution ($m^{e\mu}$ or $\Delta\phi^{e\mu}$), one has

$$\rho_{ij} = \delta_i \delta_j \left(\delta_{ij} - \frac{2N_i N_j}{N^2} \right), \quad (2.2)$$

i.e. an anti-correlation. With this at hand, we can calculate the χ^2 for the different SM predictions given by ATLAS, see Table 1, in the standard way.⁵

Next, we can inject an arbitrary NP signal which we normalize to the corresponding total NP cross-section as well as the (normalized) SM cross-section. This means for each (normalized) value of bin i of a given distribution we add a normalized cross-section of

$$r_i = \frac{\sigma_i^{\text{NP}}/\sigma^{\text{NP}}}{\sigma_i^{\text{SM}}/\sigma^{\text{SM}}}, \quad (2.3)$$

with $\sum_i \sigma_i^{\text{NP,SM}} = \sigma^{\text{NP,SM}}$. We can now calculate the χ^2 including the NP contribution. Treating NP linearly as a small perturbation we have

$$\chi_{\text{NP}}^2 = \sum_{i,j=1} (ax_i + \epsilon_{\text{NP}} r_i - 1) \rho_{ij}^{-1} (ax_j + \epsilon_{\text{NP}} r_j - 1). \quad (2.4)$$

In order to find the best fit, the χ^2 function is minimized with respect to ϵ_{NP} and a (i.e. the fitting parameters of the χ^2 distribution), the latter taking into account the possible

⁴Note that also the NNLO corrections of Refs. [60, 61] are not capable of bringing SM and data in the low $m^{e\mu}$ region into agreement but improve the agreement at high $m^{e\mu}$ where our NP models does not contribute.

⁵Due to the lack of information, we assumed the systematic errors to have the same correlations as the statistical ones meaning that we applied the correlation matrix to the full error given in the ATLAS tables. Therefore, and due to the digitization accuracy, our values slightly differ from the ones given in the ATLAS paper. However, the impact on the relevant $\Delta\chi^2$ values calculated with a NP hypothesis is expected to be small.

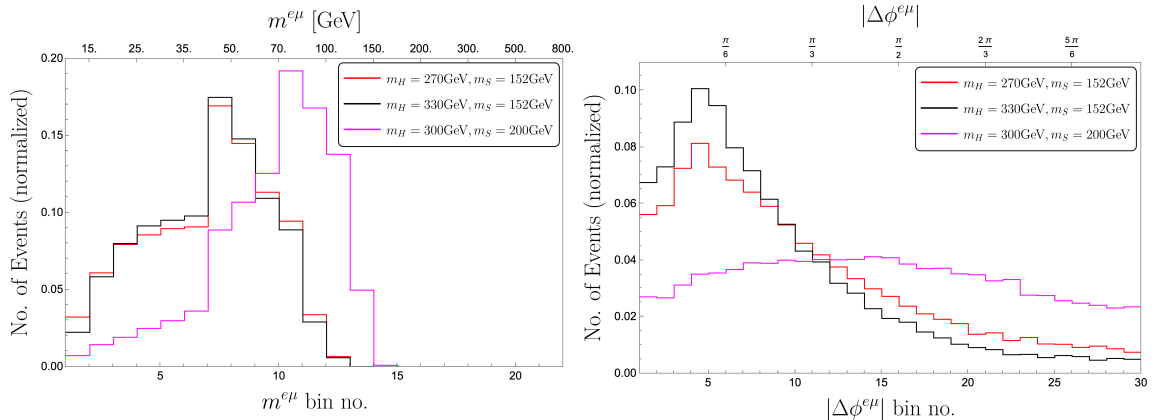


Figure 3. Number of normalized events of the NP process $pp \rightarrow H \rightarrow SS' \rightarrow WWbb$ in the bins of $m^{e\mu}$ (left) and $|\Delta\phi^{e\mu}|$ (right) for three choices of masses: $m_H = 270$ GeV, $m_S = 152$ GeV; $m_H = 330$ GeV, $m_S = 152$ GeV; $m_H = 300$ GeV, $m_S = 200$ GeV; while fixing $m_{S'} = 95$ GeV. The NP distribution appears nearly independent of m_H and is primarily affected by m_S .

rescaling of the total cross-section (as done in the ATLAS analysis). Importantly, this means that even if the NP contribution is localized at low $m^{e\mu}$ or $|\Delta\phi^{e\mu}|$ values, higher values are affected since the (predicted) values of x_i are lowered for a non-vanishing NP effect. The values of r_i must now be determined from a NP and SM simulation and the total NP cross-section can be approximated by

$$\sigma_{\text{NP}} \approx \epsilon_{\text{NP}} \sum_i r_i \sigma_i^{\text{EXP}}, \quad (2.5)$$

if NP is a small correction to the SM.⁶

3 Simplified Model Analysis

Let us now consider a simplified model in which H is produced via gluon fusion and decays into two lighter scalars S and S' which subsequently decay to WW and $b\bar{b}$, respectively.⁷ We use the hints for di-photon resonances to fix $m_S = 152$ GeV (for now) and $m_{S'} = 95$ GeV and assume $m_H > m_S + m_{S'}$ such that an on-shell decay is possible. For concreteness, we will fix $m_H = 270$ GeV, as suggested in Ref. [28] as a benchmark point, but we checked that varying its mass has a negligible impact on the fit as shown in Fig. 3.

We simulated in this setup the process $pp \rightarrow H \rightarrow SS' \rightarrow (WW^{(*)}) \rightarrow \ell^+ \nu \ell^- \nu \bar{b} \bar{b}$, with $\ell = e, \mu, \tau$, and the tau lepton subsequently decaying, using `MadGraph5aMC@NLO` [54], `Pythia8.3` [53], and `Delphes` [63]. Note that since our NP contribution is a small perturbation compared to the SM cross-section, the dependence of it on the MC generators

⁶Note that ϵ_{NP} is only used as a fitting parameter while the results are given in terms of σ_{NP} , which is equivalent.

⁷Note that this is naturally the case if S is a SM-like Higgs and S' is the neutral component of an $SU(2)_L$ triplet with hypercharge 0.

used is small. This now determines the shape of the NP contribution to the differential lepton distributions. As outlined in the introduction, we will focus on $m^{e\mu}$ and $|\Delta\phi^{e\mu}|$, including the correlations among them as described in the previous section. The results are shown as solid lines in Fig. 2. One can see that for all SM simulations used by ATLAS, the agreement with data is significantly improved. In fact, as given in Table. 1, the χ^2 is reduced between $\Delta\chi^2 = 34$ and $\Delta\chi^2 = 158$, corresponding to a preference of the NP model over the SM hypothesis by 5.8σ – 13.0σ while the average of the SM predictions results in 9.6σ . In the appendix, we use the best-fit points for the various SM predictions and their combination to predict the differential distributions. We find in Fig. 5 that while also here the agreement with data is improved, the effect (reduction of the χ^2) is much less significant than for $m^{e\mu}$ and $|\Delta\phi^{e\mu}|$, justifying our choice of input for the global fit.

So far, we fixed the masses of S and S' by using the hints for narrow di-photon resonances and took $m_H = 270$ GeV as a benchmark point which avoids constraints from SUSY and non-resonant di-Higgs searches. Let us now discuss the dependence on the masses. First of all, we checked that the effect of changing either the mass of H or of S' is very small⁸ which we show in Fig. 3. This means that one can pick any value for m_H so that this does not need to be counted as a degree of freedom in the statistical analysis. Now we can find the best-fit value in the m_S - ϵ_{NP} plane by averaging the x_i values of the six different MC simulations. For this, we generated 500k events each for m_S between 140 GeV and 160 GeV in 2 GeV steps and interpolated. As one can see from the red region in Fig. 4 the preferred 1σ range, w.r.t. the best-fit point using two degrees of freedom, for m_S is approximately 144 GeV – 157 GeV, which is perfectly consistent with a mass of 152 GeV as suggested by the di-photon excess as around 152 GeV [22].

Finally, let us consider the consistency of the preferred signal strength for $pp \rightarrow H \rightarrow SS'$ with the di-photon excess at 95 GeV. For this, we first fix $\sigma(pp \rightarrow H \rightarrow SS')$ using the preferred NP cross-section for $WWbb$ from the average of the MC simulation leading to

$$\sigma(pp \rightarrow H \rightarrow SS') = \frac{\sigma(pp \rightarrow H \rightarrow WWb\bar{b})}{\text{Br}(S' \rightarrow b\bar{b})\text{Br}(S \rightarrow WW)} \approx \frac{9 \text{ pb}}{\text{Br}(S' \rightarrow b\bar{b})\text{Br}(S \rightarrow WW)}. \quad (3.1)$$

Then assume that S' is SM-like⁹ and that S decays to $\approx 100\%$ to WW . We can now calculate the di-photon signal strength of the 95 GeV Higgs in our model

$$\mu_{\gamma\gamma}^{\text{NP}} = \frac{\sigma(pp \rightarrow H \rightarrow SS'_{\text{SM}})\text{Br}(S'_{\text{SM}} \rightarrow \gamma\gamma)}{\sigma(pp \rightarrow h_{95})\text{Br}(h_{95} \rightarrow \gamma\gamma)} \approx 0.15 \quad (3.2)$$

where h_{95} represents a hypothetical Higgs boson with a mass of 95 GeV¹⁰. Comparing this to the experimental value of $\mu_{\gamma\gamma} = 0.24_{-0.08}^{+0.09}$ [65], one can see in Fig. 4 that the predicted signal strength using the $t\bar{t}$ differential distributions (red) is perfectly consistent with the

⁸Note that while the effect on the determined NP contribution to the cross section is small since the efficiencies do not depend strongly on m_H , the gluon fusion production cross section of H falls with increasing mass. However, this effect can be e.g. absorbed into its top Yukawa coupling in the case of the UV complete model outlined in Sec. 4

⁹The branching ratio to photons of a SM-like Higgs with a mass of 95 GeV is $\approx 1.4 \times 10^{-3}$ while the one to $b\bar{b}$ is ≈ 0.86 [64] and the production cross section at 13 TeV via gluon fusion is ≈ 68 pb [64].

¹⁰Notice that this means $\text{Br}(S'_{\text{SM}} \rightarrow \gamma\gamma) = \text{Br}(h_{95} \rightarrow \gamma\gamma)$

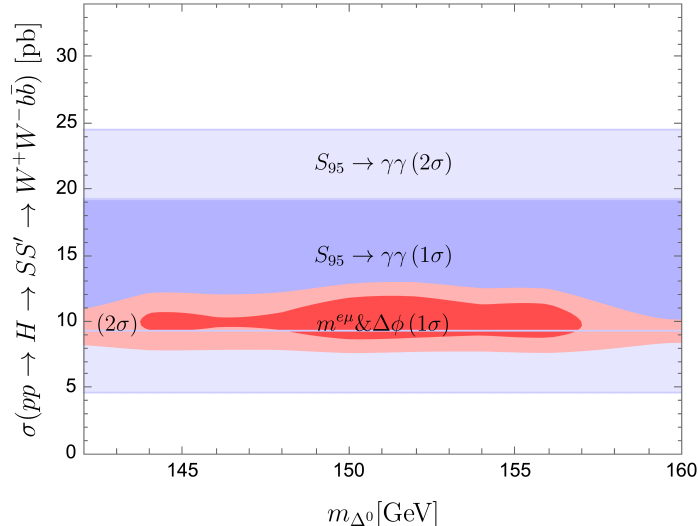


Figure 4. Preferred regions from the $t\bar{t}$ differential distributions obtained from the average of the MC simulations, i.e. 9pb, (red) as a function of m_S and the total cross section $pp \rightarrow H \rightarrow SS' \rightarrow WWb\bar{b}$ assuming S' to be SM-like and $\text{Br}[S \rightarrow WW] = 100\%$. The blue region is preferred by the 95 GeV $\gamma\gamma$ signal strength at 1σ and 2σ .

region preferred by the di-photon excess at 95 GeV (blue) in our simplified model. For this prediction, we assumed $\text{Br}(S \rightarrow WW) \approx 100\%$. Note that while in a UV complete model, one cannot expect that S decays only to WW , if the mixing angle α of the neutral triplet component with the SM Higgs is small this decay is dominant.¹¹

4 Conclusions

ATLAS found that the measured differential lepton distributions in its $t\bar{t}$ analysis significantly deviate from the SM predictions obtained for different combinations of simulators: “No model (SM simulation) can describe all measured distributions within their uncertainties.” Taking into account the performance of the ATLAS detector w.r.t. leptons and the level of sophistication of the SM simulations, this suggests that the measurement is contaminated by NP contributions.

In this article, we propose that the process $pp \rightarrow H \rightarrow SS' \rightarrow WWb\bar{b}$ constitutes a NP background to the measurements of $t\bar{t}$ differential lepton distributions. Motivated by the hints for di-photon resonances ≈ 95 GeV and ≈ 152 GeV we considered the benchmark point with S' and S having the corresponding masses and decaying to $b\bar{b}$ and WW , respectively (with $m_H = 270$ GeV). We find that this NP hypothesis is preferred over the SM one by 5.8σ to 13σ , depending on which of the six SM simulations employed by ATLAS is considered. In fact, all differential distributions, in particular $m^{e\mu}$ and $|\Delta\phi^{e\mu}|$, are much

¹¹To be more specific if $-0.05 < \alpha < 0.02$, $\text{Br}(S \rightarrow WW) > 90\%$ for a triplet vacuum expectation value of 3.4 GeV [66].

	S'	H_1	H_2	Δ
$SU(2)_L$	1	2	2	3
$U(1)_Y$	0	1/2	1/2	0
Z_2^1	+	-	+	-
Z_2^2	-	+	-	+
components	S'	H, A, H^\pm	h, G^0, G^\pm	S, Δ^\pm

Table 2. Fields and their components in the limit of vanishing mixing angles. h , S and S' correspond to SM Higgs, triplet Higgs with mass of ≈ 150 GeV, and singlet Higgs with mass 95 GeV, respectively. G^0 and G^\pm are the Goldstone bosons while CP -even H and CP -odd A originate from H_1 and have masses around 300 GeV and 400 GeV, respectively. Finally, also H^\pm could have a mass around 400 GeV.

better described once NP is included and averaging the SM predictions a significance of 9.6σ is found.

Varying m_S , to which the distributions are most sensitive among the new scalar masses, we showed that the preferred range is compatible with $m_S \approx 152$ GeV, as motivated by the $\gamma\gamma$ and WW excesses. Since the latter analysis employs a jet veto, this further disfavours the possibility that higher-order QCD corrections are the origin of the tension in the $t\bar{t}$ differential distributions. Furthermore, averaging the six different SM predictions $\sigma(pp \rightarrow H \rightarrow SS' \rightarrow WWb\bar{b}) \approx 9\text{pb}$ is preferred by $t\bar{t}$ data. Assuming that S' is SM-like, this results in a di-photon signal strength in agreement with the $\gamma\gamma$ excess. This provides further support for the emerging excess at ≈ 95 GeV which naturally has a large $b\bar{b}$ branching ratio and opens a window of opportunity to further explore this boson in associated production.

Finally, we notice that for S a dominant decay to W bosons is needed while the ZZ rate should be low to respect the limits from inclusive 4ℓ searches. This suggests that S is the neutral component of the $SU(2)_L$ triplet with hypercharge 0 (Δ), as also motivated by the W -mass average. In fact, a possible model giving the phenomenology described above is a two-Higgs-doublets model (with the Higgs doublets H_1 and H_2) supplemented by a triplet with hypercharge 0 (Δ) and a singlet (S'), as shown in Table 2. For completeness, let us write the lagrangian sector involving the scalars. As in the 2HDMS, one can employ two Z_2 symmetries, one (Z_2^1) under which S' and H_2 are odd, and one (Z_2^2) under which H_1 and Δ are odd, while all other fields are even apart from the right-handed fermions. These Z_2 symmetries allow only for Yukawa couplings of H_2 and constrain the scalar potential to be

$$\begin{aligned}
\mathcal{L}_{\text{scalar}} = & -\mu_1|H_1|^2 - \mu_2|H_2|^2 - (\mu_3 H_1^\dagger H_2 + \text{h.c.}) - \mu_4 \text{Tr}[\Delta^2] - \mu_5 S'^2 + \lambda_1 |H_1|^4 + \lambda_2 |H_2|^4 \\
& + \lambda_3 \text{Tr}[\Delta^4] + \lambda_4 S'^4 + \lambda_5 |H_1|^2 |H_2|^2 + \lambda_6 H_1^\dagger H_2 H_2^\dagger H_1 + \lambda_7 ((H_1^\dagger H_2)^2 + \text{h.c.}) + \lambda_8 |H_1|^2 S'^2 \\
& + \lambda_9 |H_2|^2 S'^2 + (\lambda_{10} |H_1|^2 + \lambda_{11} |H_2|^2) \text{Tr}[\Delta^2] + \lambda_{13} \text{Tr}[\Delta^2] S'^2 + (\kappa H_1^\dagger \Delta H_2 S' + \text{h.c.}).
\end{aligned} \tag{4.1}$$

The last term, namely the one proportional to κ , can generate the desired associated production of S and S' if H (contained in H_1) is produced via gluon fusion, e.g. via a top quark loop. We therefore assume that the Z_2 symmetries are broken in the top sector by the term

$$-\mathcal{L}_Y^{Z_2} = \mu_t \sqrt{2} \frac{m_t}{v} \bar{Q}_3 \tilde{H}_1 u_3. \quad (4.2)$$

Furthermore, since $v_\Delta, v_1 \ll v_2$ (where v_Δ, v_1, v_2 are the vacuum expectation values of Δ, H_1 and H_2 , respectively), this naturally leads to a small mixing with the SM-like Higgs (contained in H_2) such that the constraints from signal strength measurements are satisfied.¹²

Acknowledgments

The work of A.C., S.B. and G.C. is supported by a professorship grant from the Swiss National Science Foundation (No. PP00P2.211002). B.M. gratefully acknowledges the South African Department of Science and Innovation through the SA-CERN program, the National Research Foundation, and the Research Office of the University of the Witwatersrand for various forms of support.

¹²This model thus contains in addition to the SM Higgs three neutral CP-even Higgses, one neutral CP-odd Higgs and a charged scalar. Note that the interactions of these fields with gauge bosons are determined by their representations under the SM gauge group. In Ref. [67], we recently investigated this model in more detail, using the results of this article from the differential $t\bar{t}$ distributions as crucial input.

A Additional Differential Distributions

In this Appendix, we present the SM and NP predictions for the four observables η , $E^e + E^\mu$, $p_T^e + p_T^\mu$ and $p_T^{e\mu}$.

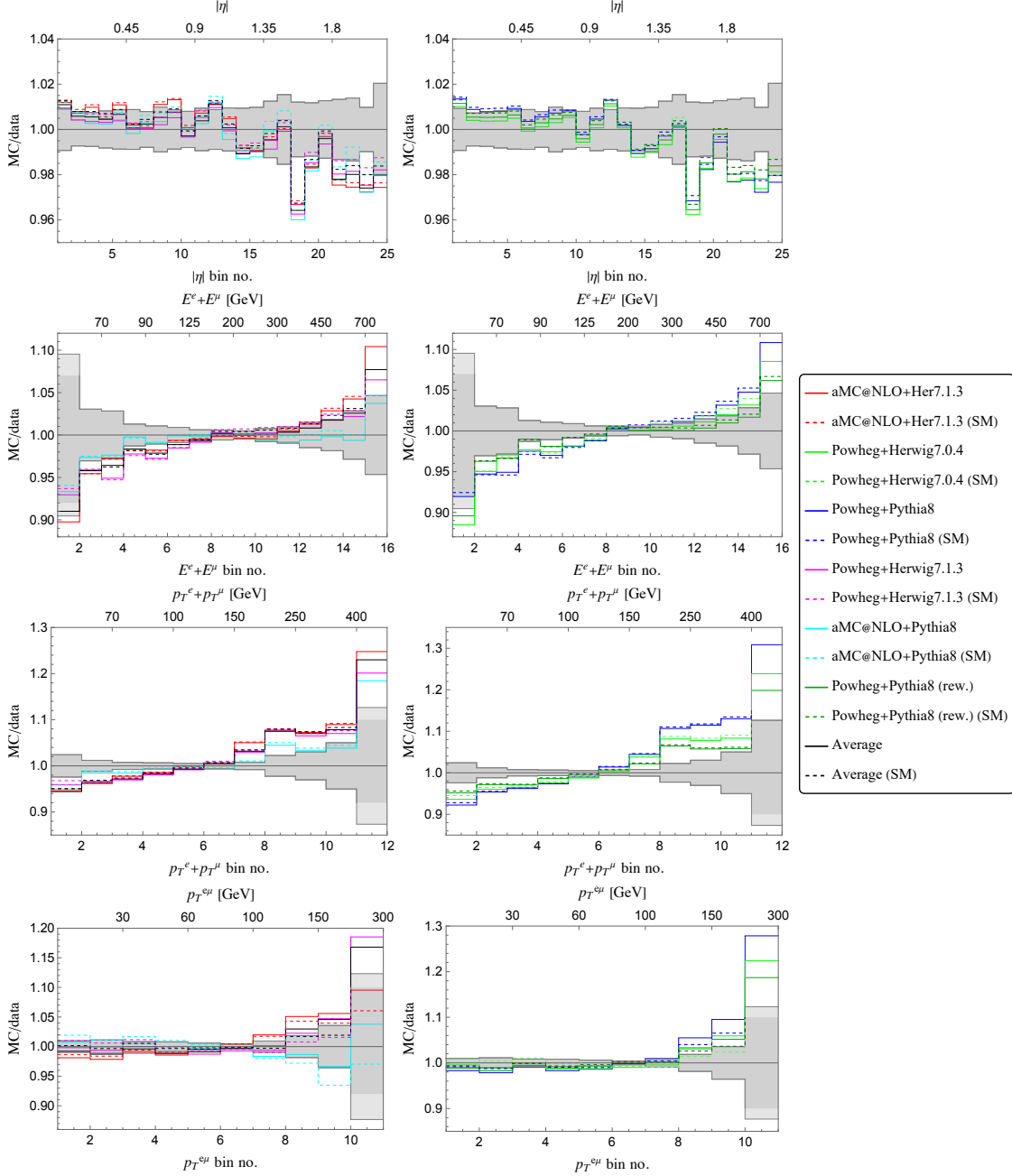


Figure 5. SM values (dashed) and NP predictions (solid), using the best fit from $m^{e\mu}$ and $|\Delta\phi^{e\mu}|$, for six other differential distributions given in the ATLAS paper and their average (black). One can see that while NP improves the agreement of theory with data, the effect is not as significant as in $m^{e\mu}$ and $|\Delta\phi^{e\mu}|$, justifying our input choice. Only $y^{e\mu}$ and $p_T^{e\mu}$ are not shown since here both the tensions within the SM as well as the NP effect are very small.

References

- [1] **Particle Data Group** Collaboration, P. A. Zyla *et al.*, “Review of Particle Physics,” *PTEP* **2020** no. 8, (2020) 083C01.
- [2] P. W. Higgs, “Broken symmetries, massless particles and gauge fields,” *Phys. Lett.* **12** (1964) 132–133.
- [3] F. Englert and R. Brout, “Broken Symmetry and the Mass of Gauge Vector Mesons,” *Phys. Rev. Lett.* **13** (1964) 321–323.
- [4] P. W. Higgs, “Broken Symmetries and the Masses of Gauge Bosons,” *Phys. Rev. Lett.* **13** (1964) 508–509.
- [5] G. S. Guralnik, C. R. Hagen, and T. W. B. Kibble, “Global Conservation Laws and Massless Particles,” *Phys. Rev. Lett.* **13** (1964) 585–587.
- [6] **ATLAS** Collaboration, G. Aad *et al.*, “Observation of a new particle in the search for the Standard Model Higgs boson with the ATLAS detector at the LHC,” *Phys. Lett. B* **716** (2012) 1–29, [arXiv:1207.7214 \[hep-ex\]](#).
- [7] **CMS** Collaboration, S. Chatrchyan *et al.*, “Observation of a New Boson at a Mass of 125 GeV with the CMS Experiment at the LHC,” *Phys. Lett. B* **716** (2012) 30–61, [arXiv:1207.7235 \[hep-ex\]](#).
- [8] **ATLAS, CMS** Collaboration, J. M. Langford, “Combination of Higgs measurements from ATLAS and CMS : couplings and \parallel - framework,” *PoS LHCP2020* (2021) 136.
- [9] **ATLAS** Collaboration, “Combined measurements of Higgs boson production and decay using up to 139 fb⁻¹ of proton-proton collision data at $\sqrt{s} = 13$ TeV collected with the ATLAS experiment,”.
- [10] **ALEPH, DELPHI, L3, OPAL, LEP Electroweak** Collaboration, S. Schael *et al.*, “Electroweak Measurements in Electron-Positron Collisions at W-Boson-Pair Energies at LEP,” *Phys. Rept.* **532** (2013) 119–244, [arXiv:1302.3415 \[hep-ex\]](#).
- [11] **LHCb** Collaboration, R. Aaij *et al.*, “Measurement of the W boson mass,” *JHEP* **01** (2022) 036, [arXiv:2109.01113 \[hep-ex\]](#).
- [12] **CDF** Collaboration, T. Aaltonen *et al.*, “High-precision measurement of the W boson mass with the CDF II detector,” *Science* **376** no. 6589, (2022) 170–176.
- [13] **ATLAS** Collaboration, “Improved W boson Mass Measurement using 7 TeV Proton-Proton Collisions with the ATLAS Detector,”.
- [14] **LHC-TeV MW Working Group** Collaboration, S. Amoroso *et al.*, “Compatibility and combination of world W-boson mass measurements,” *Eur. Phys. J. C* **84** no. 5, (2024) 451, [arXiv:2308.09417 \[hep-ex\]](#).
- [15] A. Strumia, “Interpreting electroweak precision data including the W-mass CDF anomaly,” *JHEP* **08** (2022) 248, [arXiv:2204.04191 \[hep-ph\]](#).
- [16] **LEP Working Group for Higgs boson searches, ALEPH, DELPHI, L3, OPAL** Collaboration, R. Barate *et al.*, “Search for the standard model Higgs boson at LEP,” *Phys. Lett. B* **565** (2003) 61–75, [arXiv:hep-ex/0306033](#).
- [17] **CMS** Collaboration, A. M. Sirunyan *et al.*, “Search for a standard model-like Higgs boson in the mass range between 70 and 110 GeV in the diphoton final state in proton-proton

- collisions at $\sqrt{s} = 8$ and 13 TeV,” *Phys. Lett. B* **793** (2019) 320–347, [arXiv:1811.08459 \[hep-ex\]](#).
- [18] **CMS** Collaboration, A. M. Sirunyan *et al.*, “Searches for additional Higgs bosons and vector leptoquarks in $\tau\tau$ final states in proton-proton collisions at $\sqrt{s} = 13$ TeV,” <http://cds.cern.ch/record/2803739>.
- [19] **CMS** Collaboration, A. M. Sirunyan *et al.*, “Search for a new resonance decaying to two scalars in the final state with two bottom quarks and two photons in proton-proton collisions at $\sqrt{s} = 13$ TeV,”.
- [20] **ATLAS** Collaboration, G. Aad *et al.*, “Search for diphoton resonances in the 66 to 110 GeV mass range using 140 fb⁻¹ of 13 TeV pp collisions collected with the ATLAS detector,”.
- [21] **ATLAS** Collaboration, G. Aad *et al.*, “Search for dark matter in events with missing transverse momentum and a Higgs boson decaying into two photons in pp collisions at $\sqrt{s} = 13$ TeV with the ATLAS detector,” *JHEP* **10** (2021) 013, [arXiv:2104.13240 \[hep-ex\]](#).
- [22] A. Crivellin, Y. Fang, O. Fischer, A. Kumar, M. Kumar, E. Malwa, B. Mellado, N. Rappheeha, X. Ruan, and Q. Sha, “Accumulating Evidence for the Associate Production of a Neutral Scalar with Mass around 151 GeV,” *accepted for publication in Phys. Rev. D* (9, 2021) , [arXiv:2109.02650 \[hep-ph\]](#).
- [23] S. Bhattacharya, G. Coloretti, A. Crivellin, S.-E. Dahbi, Y. Fang, M. Kumar, and B. Mellado, “Growing Excesses of New Scalars at the Electroweak Scale,” [arXiv:2306.17209 \[hep-ph\]](#).
- [24] S. Buddenbrock, A. S. Cornell, Y. Fang, A. Fadol Mohammed, M. Kumar, B. Mellado, and K. G. Tomiwa, “The emergence of multi-lepton anomalies at the LHC and their compatibility with new physics at the EW scale,” *JHEP* **10** (2019) 157, [arXiv:1901.05300 \[hep-ph\]](#).
- [25] S. von Buddenbrock, R. Ruiz, and B. Mellado, “Anatomy of inclusive $t\bar{t}W$ production at hadron colliders,” *Phys. Lett. B* **811** (2020) 135964, [arXiv:2009.00032 \[hep-ph\]](#).
- [26] Y. Hernandez, M. Kumar, A. S. Cornell, S.-E. Dahbi, Y. Fang, B. Lieberman, B. Mellado, K. Monnakgotla, X. Ruan, and S. Xin, “The anomalous production of multi-lepton and its impact on the measurement of Wh production at the LHC,” *Eur. Phys. J. C* **81** no. 4, (2021) 365, [arXiv:1912.00699 \[hep-ph\]](#).
- [27] O. Fischer *et al.*, “Unveiling hidden physics at the LHC,” *Eur. Phys. J. C* **82** no. 8, (2022) 665, [arXiv:2109.06065 \[hep-ph\]](#).
- [28] S. von Buddenbrock, A. S. Cornell, A. Fadol, M. Kumar, B. Mellado, and X. Ruan, “Multi-lepton signatures of additional scalar bosons beyond the Standard Model at the LHC,” *J. Phys. G* **45** no. 11, (2018) 115003, [arXiv:1711.07874 \[hep-ph\]](#).
- [29] G. Coloretti, A. Crivellin, S. Bhattacharya, and B. Mellado, “Searching for Low-Mass Resonances Decaying into W Bosons,” [arXiv:2302.07276 \[hep-ph\]](#).
- [30] **ATLAS** Collaboration, G. Aad *et al.*, “Inclusive and differential cross-sections for dilepton $t\bar{t}$ production measured in $\sqrt{s} = 13$ TeV pp collisions with the ATLAS detector,” *JHEP* **07** (2023) 141, [arXiv:2303.15340 \[hep-ex\]](#).
- [31] M. Beneke, P. Falgari, S. Klein, and C. Schwinn, “Hadronic top-quark pair production with NNLL threshold resummation,” *Nucl. Phys. B* **855** (2012) 695–741, [arXiv:1109.1536 \[hep-ph\]](#).

- [32] P. Bärnreuther, M. Czakon, and A. Mitov, “Percent Level Precision Physics at the Tevatron: First Genuine NNLO QCD Corrections to $q\bar{q} \rightarrow t\bar{t} + X$,” *Phys. Rev. Lett.* **109** (2012) 132001, [arXiv:1204.5201 \[hep-ph\]](#).
- [33] M. Czakon and A. Mitov, “NNLO corrections to top-pair production at hadron colliders: the all-fermionic scattering channels,” *JHEP* **12** (2012) 054, [arXiv:1207.0236 \[hep-ph\]](#).
- [34] N. Kidonakis and C. Foster, “Soft-gluon corrections in $t\bar{t}W$ production,” [arXiv:2312.00861 \[hep-ph\]](#).
- [35] **ATLAS** Collaboration, M. Aaboud *et al.*, “Measurement of lepton differential distributions and the top quark mass in $t\bar{t}$ production in pp collisions at $\sqrt{s} = 8$ TeV with the ATLAS detector,” *Eur. Phys. J. C* **77** no. 11, (2017) 804, [arXiv:1709.09407 \[hep-ex\]](#).
- [36] **ATLAS** Collaboration, G. Aad *et al.*, “Measurement of the $t\bar{t}$ production cross-section and lepton differential distributions in $e\mu$ dilepton events from pp collisions at $\sqrt{s} = 13$ TeV with the ATLAS detector,” *Eur. Phys. J. C* **80** no. 6, (2020) 528, [arXiv:1910.08819 \[hep-ex\]](#).
- [37] **CMS** Collaboration, A. M. Sirunyan *et al.*, “Measurements of $t\bar{t}$ differential cross sections in proton-proton collisions at $\sqrt{s} = 13$ TeV using events containing two leptons,” *JHEP* **02** (2019) 149, [arXiv:1811.06625 \[hep-ex\]](#).
- [38] **CMS** Collaboration, A. M. Sirunyan *et al.*, “Measurement of the top quark Yukawa coupling from $t\bar{t}$ kinematic distributions in the dilepton final state in proton-proton collisions at $\sqrt{s} = 13$ TeV,” *Phys. Rev. D* **102** no. 9, (2020) 092013, [arXiv:2009.07123 \[hep-ex\]](#).
- [39] **CMS** Collaboration, A. M. Sirunyan *et al.*, “Measurement of the production cross section for single top quarks in association with W bosons in proton-proton collisions at $\sqrt{s} = 13$ TeV,” *JHEP* **10** (2018) 117, [arXiv:1805.07399 \[hep-ex\]](#).
- [40] **ATLAS** Collaboration, G. Aad *et al.*, “The ATLAS Simulation Infrastructure,” *Eur. Phys. J. C* **70** (2010) 823–874, [arXiv:1005.4568 \[physics.ins-det\]](#).
- [41] **CMS** Collaboration, A. M. Sirunyan *et al.*, “Extraction and validation of a new set of CMS PYTHIA8 tunes from underlying-event measurements,” *Eur. Phys. J. C* **80** no. 1, (2020) 4, [arXiv:1903.12179 \[hep-ex\]](#).
- [42] **ATLAS** Collaboration, G. Aad *et al.*, “Electron and photon performance measurements with the ATLAS detector using the 2015–2017 LHC proton-proton collision data,” *JINST* **14** no. 12, (2019) P12006, [arXiv:1908.00005 \[hep-ex\]](#).
- [43] **CMS** Collaboration, V. Khachatryan *et al.*, “Performance of Electron Reconstruction and Selection with the CMS Detector in Proton-Proton Collisions at $\sqrt{s} = 8$ TeV,” *JINST* **10** no. 06, (2015) P06005, [arXiv:1502.02701 \[physics.ins-det\]](#).
- [44] **CMS** Collaboration, S. Chatrchyan *et al.*, “Performance of CMS Muon Reconstruction in pp Collision Events at $\sqrt{s} = 7$ TeV,” *JINST* **7** (2012) P10002, [arXiv:1206.4071 \[physics.ins-det\]](#).
- [45] **CMS** Collaboration, A. Tumasyan *et al.*, “Measurements of the Higgs boson production cross section and couplings in the W boson pair decay channel in proton-proton collisions at $\sqrt{s} = 13$ TeV,” *Eur. Phys. J. C* **83** no. 7, (2023) 667, [arXiv:2206.09466 \[hep-ex\]](#).
- [46] **ATLAS** Collaboration, “Measurements of Higgs boson production by gluon–gluon fusion and vector-boson fusion using $H \rightarrow WW^* \rightarrow e\nu\mu\nu$ decays in pp collisions at $\sqrt{s} = 13$ TeV with the ATLAS detector,” [arXiv:2207.00338 \[hep-ex\]](#).

- [47] T. Ježo, J. M. Lindert, and S. Pozzorini, “Resonance-aware NLOPS matching for off-shell $t\bar{t} + tW$ production with semileptonic decays,” [arXiv:2307.15653 \[hep-ph\]](#).
- [48] S. Frixione, P. Nason, and C. Oleari, “Matching NLO QCD computations with Parton Shower simulations: the POWHEG method,” *JHEP* **11** (2007) 070, [arXiv:0709.2092 \[hep-ph\]](#).
- [49] S. Alioli, P. Nason, C. Oleari, and E. Re, “A general framework for implementing NLO calculations in shower Monte Carlo programs: the POWHEG BOX,” *JHEP* **06** (2010) 043, [arXiv:1002.2581 \[hep-ph\]](#).
- [50] S. Frixione, P. Nason, and G. Ridolfi, “A Positive-weight next-to-leading-order Monte Carlo for heavy flavour hadroproduction,” *JHEP* **09** (2007) 126, [arXiv:0707.3088 \[hep-ph\]](#).
- [51] **NNPDF** Collaboration, R. D. Ball *et al.*, “Parton distributions for the LHC Run II,” *JHEP* **04** (2015) 040, [arXiv:1410.8849 \[hep-ph\]](#).
- [52] T. Sjöstrand, S. Mrenna, and P. Z. Skands, “PYTHIA 6.4 Physics and Manual,” *JHEP* **05** (2006) 026, [arXiv:hep-ph/0603175](#).
- [53] T. Sjöstrand, S. Ask, J. R. Christiansen, R. Corke, N. Desai, P. Ilten, S. Mrenna, S. Prestel, C. O. Rasmussen, and P. Z. Skands, “An introduction to PYTHIA 8.2” *Comput. Phys. Commun.* **191** (2015) 159–177, [arXiv:1410.3012 \[hep-ph\]](#).
- [54] J. Alwall, R. Frederix, S. Frixione, V. Hirschi, F. Maltoni, O. Mattelaer, H. S. Shao, T. Stelzer, P. Torrielli, and M. Zaro, “The automated computation of tree-level and next-to-leading order differential cross sections, and their matching to parton shower simulations,” *JHEP* **07** (2014) 079, [arXiv:1405.0301 \[hep-ph\]](#).
- [55] R. D. Ball *et al.*, “Parton distributions with LHC data,” *Nucl. Phys. B* **867** (2013) 244–289, [arXiv:1207.1303 \[hep-ph\]](#).
- [56] M. Bahr *et al.*, “Herwig++ Physics and Manual,” *Eur. Phys. J. C* **58** (2008) 639–707, [arXiv:0803.0883 \[hep-ph\]](#).
- [57] J. Bellm *et al.*, “Herwig 7.0/Herwig++ 3.0 release note,” *Eur. Phys. J. C* **76** no. 4, (2016) 196, [arXiv:1512.01178 \[hep-ph\]](#).
- [58] J. Bellm *et al.*, “Herwig 7.1 Release Note,” [arXiv:1705.06919 \[hep-ph\]](#).
- [59] M. Czakon, D. Heymes, A. Mitov, D. Pagani, I. Tsinikos, and M. Zaro, “Top-pair production at the LHC through NNLO QCD and NLO EW,” *JHEP* **10** (2017) 186, [arXiv:1705.04105 \[hep-ph\]](#).
- [60] A. Behring, M. Czakon, A. Mitov, A. S. Papanastasiou, and R. Poncelet, “Higher order corrections to spin correlations in top quark pair production at the LHC,” *Phys. Rev. Lett.* **123** no. 8, (2019) 082001, [arXiv:1901.05407 \[hep-ph\]](#).
- [61] M. Czakon, A. Mitov, and R. Poncelet, “NNLO QCD corrections to leptonic observables in top-quark pair production and decay,” *JHEP* **05** (2021) 212, [arXiv:2008.11133 \[hep-ph\]](#).
- [62] A. Rohatgi, “Webplotdigitizer: Version 4.6.” 2022. <https://automeris.io/WebPlotDigitizer>.
- [63] **DELPHES 3** Collaboration, J. de Favereau, C. Delaere, P. Demin, A. Giammanco, V. Lemaître, A. Mertens, and M. Selvaggi, “DELPHES 3, A modular framework for fast simulation of a generic collider experiment,” *JHEP* **02** (2014) 057, [arXiv:1307.6346 \[hep-ex\]](#).

- [64] **LHC Higgs Cross Section Working Group** Collaboration, D. de Florian *et al.*, “Handbook of LHC Higgs Cross Sections: 4. Deciphering the Nature of the Higgs Sector,” [arXiv:1610.07922](#) [[hep-ph](#)].
- [65] T. Biekötter, S. Heinemeyer, and G. Weiglein, “The 95.4 GeV di-photon excess at ATLAS and CMS,” [arXiv:2306.03889](#) [[hep-ph](#)].
- [66] S. Ashanujjaman, S. Banik, G. Coloretti, A. Crivellin, S. P. Maharathy, and B. Mellado, “Anatomy of the Real Higgs Triplet Model,” [arXiv:2411.18618](#) [[hep-ph](#)].
- [67] G. Coloretti, A. Crivellin, and B. Mellado, “Combined Explanation of LHC Multi-Lepton, Di-Photon and Top-Quark Excesses,” *Phys. Rev. D* **110** no. 7, (2024) 073001, [arXiv:2312.17314](#) [[hep-ph](#)].